Chapter 9
Fiber Optic Technology for Environmental Monitoring: State of the Art and Application in the Observatory of Transfers in the Vadose Zone-(O-ZNS)

B. Abbar, A. Isch, K. Michel, M. Abbas, H. Vincent, P. Abbasimaedeh, and M. Azaroual

Abstract The structure and dynamics of the Vadose Zone (VZ) play a major role in the groundwater recharge process and in the transport of contaminants. By monitoring the mass and heat transfer processes within the VZ, it will be possible to predict the contaminants travel time and implement suitable solutions to preserve the groundwater resources. Several environmental monitoring solutions have been developed in recent years to better understand the complex hydrogeological processes that occur along the VZ. The use of Fiber Optic (FO) sensors is a promising technology for environmental monitoring. Compared to conventional sensors, the FO sensors allow measuring and monitoring different parameters, while offering interesting specificities. To improve our knowledge on the reactive processes occurring during mass and heat transfers within the VZ of the Beauce aquifer, the Observatory of transfers in the VZ is being developed near Orléans (France). Three types of distributed FO

B. Abbar (✉) · A. Isch · M. Abbas · M. Azaroual
University of Orléans, CNRS, BRGM, ISTO, UMR 7327, 45071 Orléans, France
e-mail: bouamama.abbar@cnrs-orleans.fr

A. Isch
e-mail: arnaud.isch@terrainnova.fr

M. Abbas
e-mail: mohamad.abbas@cnrs-orleans.fr

M. Azaroual
e-mail: m.azaroual@brgm.fr

K. Michel · M. Azaroual
BRGM, French Geological Survey, 45060 Orléans, France
e-mail: k.michel@brgm.fr

H. Vincent · P. Abbasimaedeh
CEMENTYS, 9 Rue Léon Blum, 91120 Palaiseau, France
e-mail: huguesvincent@cementys.com

P. Abbasimaedeh
e-mail: pouyanabbasi@cementys.com

sensors (DTS, DSS and DAS) have been installed at the O-ZNS experimental site in July 2020. This chapter presents the state of the art on the use of FO sensors for environmental monitoring. The installation of these sensors at the O-ZNS site is then discussed along with the future developments and targeted results.

Keywords Fiber optics · Monitoring · Vadose zone · Groundwater · Contaminant transfer

9.1 Introduction

The Vadose Zone (VZ) is a three-phase (water–air–solid) medium spanning from the surface of the soil down to the aquifer, and is considered as a place of intense and complex exchange and transfer of mass and heat [1, 2]. The vadose zone structure plays an important role in the groundwater recharge process, as well as in the transport of contaminants through the potential development of preferential flow paths and storage reservoirs. Monitoring and understanding the VZ dynamics and physicochemical processes is of utmost importance in predicting the fate of contaminants, and in implementing suitable solutions that can help protect groundwater resources and tackle environmental concerns.

Since the 1950s, contaminations related to intensive agricultural activities have been highlighted in different hydrosystems around the world [3]. Since this period, the nitrate and pesticides contents in groundwater have increased linearly and drastically [4]. Due to growing concern among local communities about the need to protect groundwater resources for drinking and agricultural purposes, a growing body of work has focused on the identification and direct characterization of flow processes within the VZ. However, these processes are still unclear today because of the difficulties implemented in acquiring direct measurements of such phenomena. In this context, the Observatory of transfers in the Vadose Zone (O-ZNS) is being implemented in an agricultural field in Villamblain (near Orléans in France). The O-ZNS project aims to understand and quantify mass and heat transfers over the long term (several decades) thanks to a large access well instrumented with coupled and multi-method environmental monitoring techniques, and surrounded by several monitoring boreholes.

Remarkable progress has been made in recent years concerning the development of new and innovative technologies for environmental monitoring. The use of Fiber Optic (FO) technologies is a promising solution for monitoring the VZ. Indeed, FO sensors provide similar functions to conventional sensors (monitoring, control, or measurement), while offering interesting specificities and potentially added value. The advantages of these sensors include the immunity to electromagnetic interferences, the measurement of several parameters, and the capabilities of remote feeding or interrogation [5]. Additionally, thanks to their high flexibility, FO sensors can provide spatial and temporal information through directly burying them in geological formations or attaching them to subsurface structures. FO sensors are capable

of recording continuously, over large distances and at a higher frequency range than traditional sensors. Or et al. [6] indicated that conventional monitoring sensors have certain limitations mainly related to their low sensitivity to low frequencies signals and require regular maintenance. These sensors are generally designed for near-surface applications and require significant additional developments or adaptations before being able to monitor the shallow subsoil (hard geological facies) over the long term. The FO technology has led to the observation of previously unobserved low frequency signals [7, 8] which can provide valuable information related to complex and highly coupled hydrogeological and geochemical processes. Some FO sensors including Fiber Bragg Sensors (FBG) and Distributed Temperature Sensors (DTS) are currently used for the monitoring of fluids flow [9, 10], hydrogeological processes [11, 12], water content, and energy exchanges along the VZ [13–15]. Infrared optical fibers based on chalcogenide glass are used as sensors for the determination of volatile organic pollutants in groundwater. The system works following the fiber evanescent wave spectroscopy (FEWS) principle. It was tested in situ, in real time, and under real field conditions [16, 17]. Distributed Acoustic Sensors (DAS) are used to monitor micro-seismic activity, record Vertical Seismic Profiles (VSP) and detect fractures [18–20]. Many studies have also highlighted the potential of the Distributed Strain Sensor (DSS) for the monitoring of mechanical deformations linked to land subsidence or landslide [21, 22], and of deformations related to swelling and erosion of VZ material [23–25]. Lu et al. [26] and Zhong et al. [27] highlighted the potential of FO sensors in the development of industrial artificial intelligence systems. Wen et al. [28], have proposed a target recognition technique based on DAS measurements with machine learning. Many researchers have used the data obtained by FO sensors in the development of predictive models dedicated to deciphering complex hydrogeological processes [29, 30]. In recent years, several FO prototypes sensors have also been developed to measure other parameters which do not directly affect the FO such as the pH [31], metallic ion concentrations of chromium [32], salinity [33], relative humidity [34, 35], and hydrogen concentration [36]. The BRGM (French Geological Survey) have developed two optical sensors prototypes dedicated to CO_2 gas measurements in collaboration with the CNRS, University of Caen, University of Rennes and the IDIL company [37, 38].

This chapter presents a state of the art of FO sensors for environmental monitoring and their installation along three boreholes at the O-ZNS experimental site. First, the fundamentals of FO technology with a brief review of the detection systems currently used in environmental monitoring are presented. In particular, the two FO sensors types: Bragg grating sensors and distributed sensors (DTS, DAS, DSS) are treated separately, where their respective advantages and limitations are discussed. We then discuss the context and the instrumentation strategy of the O-ZNS project and present the installation of the distributed FO sensors at the O-ZNS experimental site.

9.2   Fiber Optic Technology: State of the Art and Environmental Applications

Fiber optic technology remains one of the greatest technological advances for the permanent monitoring design in recent years [39–41]. It doesn't have the disadvantages of conventional detection methods (power, impedance, sensitivity to electromagnetic fields), while allowing access to long distance measurements. FO technology offers very high bandwidth with high transmission speed.

FO is a glass cylinder that guides the light in its core (optical waveguide), by the principle of total internal reflection [39, 42]. In some cases, the core of the fiber is made of silicon oxide (SiO_2), surrounded by an optical cladding (125 μm) that is made of lower quality silica (Fig. 9.1a). The whole is protected by a third layer composed of a polymer coating (250 μm, cf. Fig. 9.1a).

There are different types of FO, including Multi-Mode (MM) and Single-Mode (SM). These different typologies make it possible to obtain different characteristics in terms of bandwidth, signal dispersion (influencing the quality of signal reception) or amplification of the optical signal. The core of the MM fiber is larger with a diameter of 50 or 62.5 μm and light signals can follow different paths depending on the angle of refraction (Fig. 9.1b) [43]. The light signals arrive at the end of the cable at different times, inducing some dispersion of the signal. In most cases, the MM fiber is reserved for smaller distance measurements (less than 10 km) compared to the SM fiber. The latter is characterized by a small diameter core (9 μm), and its light signal follows a single mode of propagation unlike the MM fiber. Consequently, the light propagation path is direct and the signal is less disturbed (Fig. 9.1c). The small diameter of the fiber core requires a significant luminous intensity, therefore expensive laser diodes, which makes the use of SM fiber more expensive compared to the MM fiber.
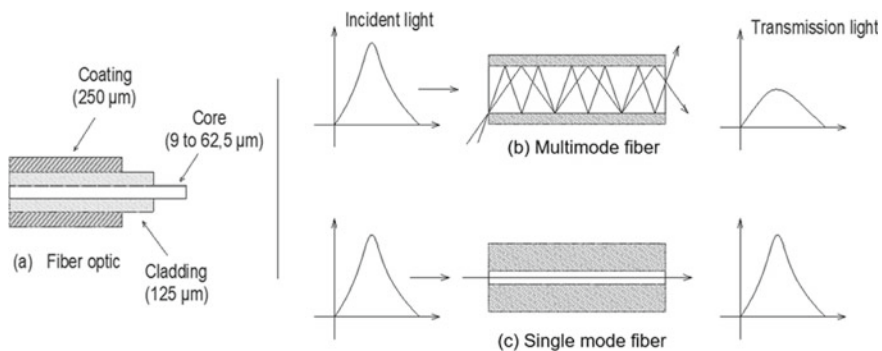
Fig. 9.1   a FO composition, **b** multi-mode FO: the light signals follow different paths depending on the angle of refraction, **c** single-mode FO: the light propagation path is direct without signal dispersion. Adapted from: [43–46]

The FO sensors are able of covering the functions of traditional sensors: monitoring, detection, and localization. Their measurement principle is based on the detection of changes in the transmitted light signal in an optical fiber. Changes in the environment around the fiber (stress, temperature or pressure) can cause variations in the transmitted signal. Different physical phenomena are used to modulate the transmitted light, which gives each sensor its characteristic performance. There are two main families of FO sensors: Fiber Bragg Grating (FBG) sensors (point measurements) and distributed sensors (continuous measurements).

9.2.1   Fiber Bragg Grating Sensors: Point Measurements

FBG sensors represent short sections of the FO that contains a modulation or a periodic variation of the refractive index (Fig. 9.2). When these sensors are lit by a coherent light, each FBG reflects a precise wavelength [47]. The reflected wavelength is measured by an optical interrogator and is sensitive to temperature and deformations variations of the FBG sensor. According to Bragg's law, established by Nobel Prize winner Sir William Lawrence Bragg in 1915, the reflected wavelength of light from the grating is defined by Lecoy [48]:

$$\lambda_B = 2\Lambda_B n_{eff} \, (\text{nm}) \tag{9.1}$$

where λ_B is the reflected Bragg wavelength (nm), n_{eff} is the effective refractive index of the fiber core and Λ_B is the period of the Bragg grating. n_{eff} and Λ_B both vary with the temperature and the strain of the fiber. When the fiber undergoes deformation or when its temperature changes, a variation in the reflected wavelength λ_B can be observed:
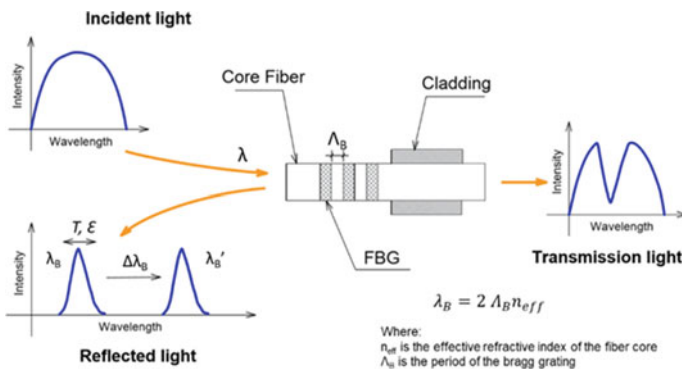
Fig. 9.2 Schematic representation of the Fiber Bragg Grating (FBG) principle. Adapted from [45, 49]

Table 9.1 Characteristics of Bragg grating FO sensor

Parameters	Value
Spatial resolution	A few millimeters ~2 mm (length of the Bragg grating)
Spatial range (L)	Up to 10 km typical (depends on link losses)
Temperature resolution	0.01 °C
Temperature range	−150 °C to up to 1000 °C
Strain resolution	0.1 µm/m
Strain range	1–4%
Number of measurement lines analyzed in parallel	10
Typical number of Bragg gratings analyzed at the measurement rate	300
Cable price[a] (from Solifos company)	5–10 €/m
FBG sensors (T/ε) price (from FTMesures and CEMENTYS company)	~375 €/sensor
FBG interrogator price (from FTMesures company)	~11 k€

Compiled from scientific publications, quotes, and data sheets
[a] Average price in Europe in 2020

$$\frac{\Delta\lambda_B}{\lambda_B} = K\varepsilon + \alpha\Delta T \qquad (9.2)$$

where the coefficient K is due to photo-elasticity (around 0.8), ε (−) is the deformation of the fiber, and ΔT (°C) is the temperature variation which expands the glass (hence the coefficient α of the order of 6.10^{-6} °C^{-1}).

The appearance of point sensors with Bragg gratings dates back to the 1990s [49]. These sensors allow the detection of pressures, deformations and temperature (Table 9.1) and the monitoring of parameters that do not directly affect the fiber (humidity, pH, salinity, etc.) [50]. These sensors can be installed directly on the soil surface to monitor deformation caused by the extraction of groundwater from an aquifer [11, 12, 51]. Alemohammad et al. [52] developed a FBG temperature and pressure sensor for soil and groundwater monitoring. This sensor was successfully tested in-situ during the thermal remediation of brownfields and the results obtained were comparable to those recorded by conventional sensors. FBG multi-parameters sensors (temperature, pressure and deformation) have been developed by Drusová et al. [51] for monitoring groundwater flow velocity. During the in-situ experiments [51], the FBG deformation sensors were installed in a field near a drinking water extraction well in Hengelo (Gelderland, Netherlands). The obtained results showed that the FBG deformation sensors were able to detect the consolidation of the VZ material caused by the extraction of groundwater in the well within a radius of 250 m. FBG sensors can also be used as extensometers to monitor natural subsidence of

soils or subsidence induced by mining. Wang et al. [53] designed micro-seismic and displacement sensors based on FBG technology. These prototypes were used in a surface subsidence monitoring system in an iron mine. According to an in-situ experiment, Huang et al. [12] have shown the feasibility of monitoring the pore water pressure profile in a borehole using FBG pressure sensors. In recent years several prototypes based on the FBG technique have been developed to detect other parameters which do not directly affect the FO such as pH, gases concentrations, heavy metals or salinity. A pH sensor based on the FBG technique in all-polymer FO was proposed by Janting et al. [31]. The sensor was coated with a layer ranging from 5 to 10 μm of pH-sensitive hydrogel. The hydrogel contracts or expands depending on the change in the pH value. The variations in pH were controlled by following the changes induced by the deformation of the fiber in the reflected Bragg wavelength λ_B. Several prototypes have been developed by adding a sensitive polymer to the FBG sensor to detect other parameters such as metallic ions of chromium [32], salinity [33, 54], relative humidity [34, 35]. Aleixandre et al. [55] proposed an FBG sensor to detect hydrogen. The FBG sensor was coated with a 5 nm layer of palladium to improve the sensitivity of silica to hydrogen. Encouraging results have been observed with a sensor response time of 10 min. The results of these studies highlight that FBG sensors provide efficient and precise measurements. Table 9.1 shows some characteristics of Bragg gratings systems.

9.2.2   Distributed FO Sensors: Continuously Sensitive

In the distributed FO sensors, the FO itself becomes the detection element and the measurement is possible at each point of the fiber. The measurement range of the distributed sensors goes from a few meters to several tens of kilometers with a metric, decametric or even centimetric resolution. Continuous, real-time measurement is nowadays a real advantage in the field of monitoring. Distributed FO sensors are used in several fields such as pipelines and wells monitoring [40, 56, 57], the oil and gas industry [58], and for monitoring several environmental parameters such as the stress, deformation, temperature, pressure, and gases concentrations [36].

Distributed FO sensors are currently attracting great interest in various fields, particularly in environmental monitoring, due to the low cost of the sensor and its fully distributed detection. However, interrogators (data analyzers) are relatively expensive compared to point sensor systems (see Tables 9.1 and 9.2). The operating principle of these sensors is based on the analysis of the light signal transmitted through the fiber: a laser sends a coherent light into the fiber of given wavelength λ_0. At all points of the fiber, the heterogeneities and the molecular vibrations of the silica will backscatter a small part of this light (Fig. 9.3a). Part of the light is returned with the same wavelength λ_0 as the incident light (Rayleigh peak). Secondary light peaks (Brillouin and Raman) are also created on both sides of the incident wavelength λ_0. Distributed FO sensors are based on three types of light-matter interactions, namely the *Rayleigh*, *Raman* and *Brillouin* backscatter phenomena. Several spectral

Table 9.2 Characteristics of distributed FO sensors

Parameters	DTS (*Raman*)	DAS (*Rayleigh*)	DSS (*Brillouin*)
Scattering mode	Raman	Rayleigh	Brillouin
Scattering categories	Inelastic	Elastic	Inelastic
Detect parameters	Temperature	Temperature/Strain (strain rates) caused by acoustic waves	Temperature/Strain
FO Requirement	Multi-mode (MM)	Single mode (SM)	Single mode (SM)
Cable recommended	Loose tube cable	Loose tube cable	Loose tube cable/Tight buffered cable
Maximal range	10 km	50 km	30 km
Spatial resolution	1 m	1–2 m	1 m
Precision	0.1 °C	0.1 °C	1 °C / 20$\mu\varepsilon$
Maximal detection frequency	–	1–50 kHz <0.1 Hz (micro-seismic)	–
Advantage	Precise measurements	Precise measurements	Stable measurements based on Brillouin frequency measurement
Disadvantage	Based on the measurement of the power amplitude, which can be disturbed in certain places of the fiber (curvature, connectors, splices)	High cost of interrogators systems generates a large volume of data (about 1 teraoctet/day of measurement)	High cost of interrogators systems
Functions	Ground water flow monitoring Thermal conductivity soil water content estimation (ADTS method)	Surfaces and crossholes seismic measurements Subsoils fracture detection (passive seismic)	Soil movement monitoring
Cable price[a] (Solifos company)	5–10 €/m	5–10 €/m	5–10 €/m
FBG interrogator price[a] (CEMENTYS company)	~50 k€	~145 k€	~80 k€

Compiled from scientific publications, quotes, and data sheets
[a] Average price in Europe in 2020
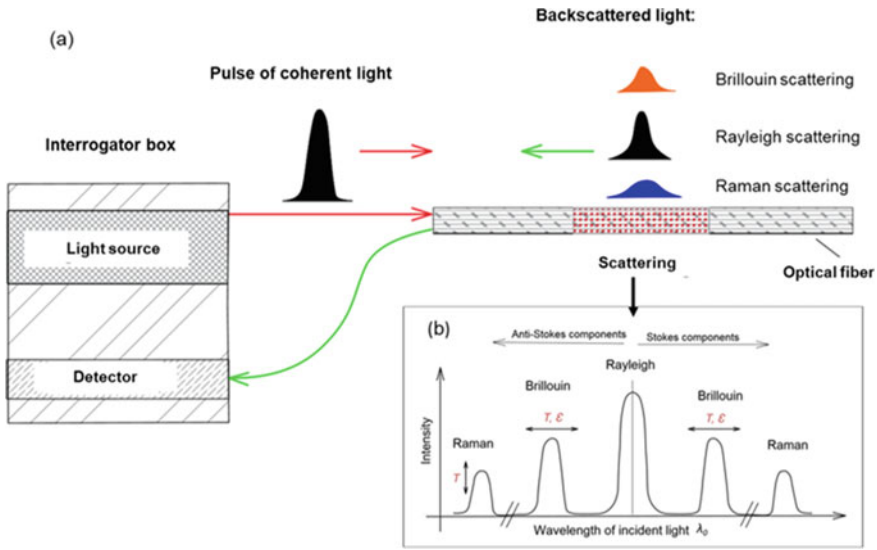
Fig. 9.3 **a** Schematic diagram of distributed FO sensors, **b** backscatter spectrum with Rayleigh, Brillouin, and Raman bands as well as the Stokes and anti-Stokes bands. Adapted from [56, 59]

components are observed in backscattering of light by silica, corresponding to these three scattering phenomena (see Fig. 9.3b).

Backscattering phenomena are classified in two categories [40]:

(i) Elastic scattering: the scattered photons keep their energy and therefore have the same frequency as the incident wave, this is the case with Rayleigh backscattering (sensitive to temperature and acoustic waves).

(ii) Inelastic scattering: photons lose (Stokes components) or gain (anti-Stokes components) energy and presents therefore a frequency (or wavelength) offset from that of the incident wave. Raman backscatter (temperature sensitive) and Brillouin backscatter (temperature and strain sensitive) are inelastic diffusions. The Raman frequency offset is around 13 THz while the Brillouin frequency offset is around 10 GHz.

These three types of scattering (*Raman*, *Brillouin* and *Rayleigh*) are shown in Fig. 9.3 and are detailed below.

Raman scattering is caused by the interaction of photons from a monochromatic light source with the molecules of the material. This results in the emission and absorption of optical phonons, with frequencies equal to the vibration frequencies of molecules in the material, of the order of ten THz. The backscattered wave then undergoes either an energy loss (Stokes wave) or an energy gain (anti-Stokes wave). Raman-based distributed temperature sensing (DTS) systems operate on the basis of the intensity ratio of the anti-Stokes component on the Stokes component of the spectrum [59, 60]:

$$R(T) = \frac{I_{a\text{-}s}}{I_s} = \left(\frac{\lambda_s}{\lambda_{a\text{-}s}}\right)^4 \exp\left(-\frac{hcv_{vib}}{kT}\right) \exp(-\Delta\alpha z) \qquad (9.3)$$

where $R(T)$ is the resulting temperature, $I_{a\text{-}s}$ is the intensity of the component of the anti-Stokes spectrum, I_s is the intensity of the component of the Stokes spectrum, λ_s is the wavelength of the component of Stokes spectrum, $\lambda_{a\text{-}s}$ is the wavelength of the component of the anti-Stokes spectrum, h is the Planck constant, c is the speed of light in a vacuum, v_{vib} is the vibration frequency, $\Delta\alpha$ is the optical attenuation between the components of the Stokes and anti-Stokes spectrum, k is the Boltzmann constant, T is the temperature and z is the head position of the FO.

Raman scattering is used to measure the temperature of the FO because the latter varies with changes in temperature. DTS uses MM fibers to measure Raman scattering and thus monitor fiber temperature (Table 9.2). Temperature sensors (DTS Raman) are used in several applications such as measuring the temperature profile in a borehole, and detecting leaks or fire events [46]. However, for Raman DTS it is necessary to use MM fibers, which represents a limit for the industry, since the measurement range is greater in SM than in MM fiber. This is the main disadvantage for these sensors in the case of long-range applications such as temperature monitoring of railways or pipelines. The Raman DTS is based on the measurement of the power amplitude and can be disturbed in certain places of the fiber (curvature, connectors, splices). DTS can also be used to monitor the thermal response of the material to the active heating of the sensing fiber [Active Heated Fiber Optics method (A-DTS)] [14, 15]. This method represents an interesting alternative to traditional sensors to monitor the variations of the water content within the VZ. The principle of A-DTS consists of heating the sensing cable with an electrically generated heat pulse and monitoring the thermal response of the VZ materials before and after the heat pulse. The resulting temperature variations can be linked to the water content of the materials [15].

Brillouin scattering comes from the interaction of light with acoustic waves (or acoustic phonons) which propagate in the fiber. It causes a frequency shift of the backscattered spectrum according to the Stokes and anti-Stokes components (Fig. 9.3). The Brillouin shift frequency depends linearly on the deformation and the temperature of the material [56]. This offset varies with the temperature changes ΔT and deformation ε of the FO according to the following equation:

$$\Delta v_B = C_T \Delta T + C_\varepsilon \varepsilon \qquad (9.4)$$

where Δv_B (Hz) is the Brillouin offset frequency, and C_T and C_ε are respectively the temperature sensitivity and deformation coefficients. They both depend on the type of FO used.

The Brillouin scattering is used to measure the temperature and the deformation of the FO. Brillouin Distributed Strain Sensing (DSS) is based on frequency measurement and uses SM fiber. Thus, the Brillouin DSS measurement is independent of the

optical loss in the fiber unlike the Raman-based DTS. However, since Brillouin scattering is both sensitive to deformation and temperature, some measurement errors can appear in one of the two parameters when the other varies.

Rayleigh scattering is caused by the interaction between an electromagnetic field which propagates in the fiber and the impurities present in the silica which modulate the refractive index [56]. This type of scattering is mainly used to assess optical losses but it has also proven its sensitivity to acoustic vibrations. Rayleigh scattering is used in Distributed Acoustic Sensing (DAS) to measure each acoustic wave surrounding a SM fiber. DAS is used in several applications such as seismic acquisition and to monitor the health of structures [18, 19, 50, 61–64].

9.2.3 Distributed Sensors Performance in the Environmental Application

Distributed detection represents a suitable solution for environmental monitoring, in particular for the detection of fractures in geological formations and for groundwater monitoring. The distributed FO sensors allow measuring the temperature and deformation over several kilometers. In recent years, a growing body of work has focused on the development of distributed FO sensors suited for environmental monitoring purposes. A multitude of researchers have studied the application and performance of these sensors [19, 56, 63, 65–67].

a. **Distributed temperature sensing (DTS)**

DTS Raman technology has been widely used in environmental monitoring [56, 58], particularly in boreholes for estimating the thermal conductivity of the VZ [68]. Unlike conventional temperature sensors, the DTS system allows continuous measurements over ranges of up to 30 km and a spatial resolution of around one meter (Table 9.3). Thanks to their low thermal mass, the sensing fibers quickly equilibrate (<1 min) to the temperature of their environment and provide measurements of the most ambient temperatures [57]. The first uses of this technique date back to the 1990s, when DTS were used to monitor geothermal energy in Mexico, Indonesia and the USA [69]. Temperature sensing for hydrogeology purposes using the DTS system dates back to the late 1990s. Hurtig et al. [70] used the DTS system to detect flow in a fractured rock along a borehole after performing hot and cold-water injections. Majorowicz and Smith [71] were among the first researchers to use the DTS technology in order to track temperature variations in the VZ when drilling a new oil well. Selker et al. [65] studied the possibility of using this technology in hydrological applications. They have shown that the DTS system can be useful for observing hydrogeological processes, including evaporation and infiltration Freifeld et al. [68] also used DTS technology in boreholes to measure the thermal conductivity of the VZ. Several studies have been carried out to better understand the capacities and limits of the DTS system [65, 72], and the validation of measurements and their

Table 9.3 An overview of recent applications of the DTS system for environmental monitoring

References	Measurements	DTS instrument	FO cable	Data collecting
[79]	Soil/rock thermal properties (surface and boreholes installation)	Ultima™ XT DTS (Silixa Ltd., UK)	FO cable (Brugg Kabel AG, Switzerland)	Sampling res.: 25 cm Temporal res.: 10–30 s Temperature res.: 0.02 °C
[64]	Soil/Rock thermal properties (boreholes installation)	DTS	MM fiber optic cable: BRUsens DTS 4.0 mm non-metallic, from Solifos—Switzerland	Installation/Calibration
[80]	Groundwater flow quantification in fractured rock boreholes	Ultima™ DTS (Silixa Ltd., UK) with a 1.8 km maximum length	A-DTS cable with diameter of 6.3 mm: from AFL FO (USA)	Sampling res.: 29 cm Temporal res.: 1 s Temperature res.: 0.01 °C
[76]	Spatial variation of the water content of sandy soil	Ultima™ DTS (Silixa Ltd., UK)	A-DTS cable: from Brug—Switzerland	Sampling res.: 0.125 m Temporal res.: 1 s
[75]	Soil water content in the surface soil	Linear Pro series DTS (AP Sensing, Böblingen, Germany) maximum measurement range of 4 km	A-DTS cable: (BRUsteel, Brugg Cable AG, Brugg, Switzerland)	Sampling res.: 0.5 m Temporal res.: 30 s
[81]	Spatio-temporal variability of groundwater discharge	Oryx DTS—Sensornet, UK	BruSteel MM cables (from Brug—Switzerland)	Sampling res.: 1 m Temporal res.: 20 min
[15]	Soil water content	Oryx DTS—Sensornet, UK	A-DTS cable: BruSteel (from Brug—Switzerland)	Heating time:120 s
[14]	Soil water content	SensorTran DTS System	A-DTS cable: BruSteel (from Brug—Switzerland)	Sampling res.: 0.5 m
[68]	Thermal conductivity/Temperature in VZ	Agilent DTS N4385A	A-DTS cable with MM fiber	Thermal measurement interval: 15 min. 64 h heating/58 h cooling
[13]	Soil moisture	DTS (maximum measurement range of 4 km)	A-DTS cable: 50/120 MM fiber	Sampling res.: 1 m Temporal res.: 40 s

calibration [73, 74]. These studies contributed to the validation of this technology and to the take-off of its use in environmental applications.

As discussed above, many researchers have investigated the potential of DTS to measure water content in the soil using A-DTS [14, 75]. The objective was to quantify the thermal response of the soil to a heat pulse over time in the form of a cumulative increase in temperature [14]:

$$T_{cum} = \int_0^{t_0} \Delta T dt \qquad (9.5)$$

where T_{cum} is the cumulative temperature increase (°C) during the total integration time t_0(s), and ΔT is the temperature change recorded by DTS compared to the ambient temperature of the materials [pre-pulse temperature (°C)].

The cumulative temperature increase (T_{cum}) during a heat pulse is a function of the thermal properties of the soil such as thermal conductivity (W/mK). The soil water content was deduced from T_{cum} using a calibration equation [14]. For a homogeneous soil, a high thermal conductivity can result in a higher water content. To relate the cumulative temperature T_{cum} and the water content, different adjustment curves were used [76]. Benítez-Buelga et al. [77] adjusted a polynomial curve connecting T_{cum} with the soil water content using the results obtained experimentally. The resulting equation is presented in Eq. (9.6):

$$T_{cum} = \frac{1}{a + bSWC + \frac{c}{SWC}} \qquad (9.6)$$

where a, b and c are numerical parameters. The R^2 of the fit curve was 0.99. Then the water content of the soil was expressed by the following relation (named SWCpoly) (Eq. 9.7):

$$Soil\ water\ content\ (SWC) = \frac{\left(\frac{1}{T_{cum}} - a\right) + \sqrt{\left(\frac{1}{T_{cum}} - a\right)^2 - 4bc}}{2b} \qquad (9.7)$$

The values of the numerical parameters are $a = 8.4 \times 10^{-5}$, $b = 2.6 \times 10^{-5}$ and $c = 1.6 \times 10^{-5}$.

The resulting temperature variations are related to the water content of the soil [14, 15]. This method has been used in recent years to monitor the groundwater flow and to measure soil water content [13]. Liu et al. [78] have used the A-DTS to detect groundwater flow in boreholes. They showed that the temperature of a heating sensor cable installed in a borehole was sensitive to the horizontal flow of groundwater through the surrounding material. Read et al. [10] also proposed a technique based on A-DTS to follow the vertical speed of fluid in boreholes using a heating sensing cable. Zubelzu et al. [76] have estimated the spatial variation of the water content of

a sandy soil in an agricultural field. The temperature data recorded by the DTS over a length of 133 m were correlated to the water content of the sandy soil using the equations described above (Eqs. 9.6 and 9.7).

All these studies have contributed to the maturation of this technology and the development of DTS systems is in constant evolution. It is now possible to measure variations of temperatures of 0.01 °C with spatial resolutions at the centimetric scale and with high frequencies. Table 9.3 summarizes recent studies made with the use of DTS sensors for environmental monitoring purposes.

b. **Distributed acoustic sensing sensors (DAS)**

The DAS technology has evolved rapidly in recent years. This new system uses a FO cable to detect acoustic frequency signals over large distances [18, 19, 61, 63, 64, 75]. The use of this technology in boreholes applications provides key information on the characteristics and geometry of fractures by monitoring variations in seismic velocity. James et al. [19] used the DAS system to detect and characterize fractures along the VZ without an active source and at a high temporal and spatial resolution. This study was conducted in a field at the Blue Canyon Dome (New Mexico). Fractures were generated by two stimulations in wells placed at the center of four monitoring wells. The FO cables were installed behind the PVC casing of the boreholes and used to record the ambient noise before and after each stimulation. The results showed a reduction of speed in the near-well area (center of the test area) and suggested the creation of fractures. This hypothesis was confirmed by tomographic images. Mellors et al. [8] conducted an exhaustive review of previous work on the use of DAS sensors in boreholes and in harsh environments. According to its synthesis, the DAS fiber sensors should be effective in boreholes applications and able to withstand high temperatures. The DAS technology has also been used for several years to carry out surface and crosshole seismic measurements. The DAS technology is increasingly used in boreholes as seismic sensors and can replace geophones. As a matter of fact, many experiments carried out at the soil surface and in boreholes have shown that this technique can be used as a good seismic sensor [20, 82–84]. Bakulin et al. [85] used the DAS system as a surface seismic sensor to carry out seismic surveys. The obtained results showed the possibility of using the DAS system as a seismic surface sensor instead of conventional accelerometers or geophones. Harris et al. [86] used the DAS system as part of the Aquistore carbon storage project (Canada) to monitor CO_2 injection into underground reservoirs (between 3.10 and 3.35 m deep). Many Vertical Seismic Profiles (VSP) were carried out with DAS and geophones to monitor the geological structure of reservoirs on the Aquistore site over time. The results obtained showed that DAS systems can provide results comparable to geophones and represents an effective alternative to traditional seismic acquisition methods.

Furthermore, the DAS technique presents many advantages over geophones because it can be carried out on the entire borehole at the same time and over several kilometers, unlike geophones which are generally deployed in short networks [82]. FO cables are easier to install temporarily or permanently in boreholes for the monitoring of the VZ. Additionally, measurements can be carried out simultaneously in

several boreholes by using a single DAS interrogator and a single FO cable. The same application with the use of geophones would require many equipment (network of geophones, recording instruments) and would also be difficult to install. However, despite these advantages, DAS technology is still under development and requires a validation of the interpretations of the measured signals and a characterization of its degree of complementarity with respect to traditional seismic measurements. Indeed, the spatial resolution issues (currently varies between 1 and 10 m) and sensitivity to environmental factors (temperature, pH, Eh, etc.) are not yet precisely determined, in particular in limestone rocks. Table 9.4 summarizes recent studies conducted with the use of DAS system for seismic measurements and fracture detection in the VZ.

c. **Distributed Strain Sensing (DSS)**

The Distributed Strain Sensing technology has emerged in recent years as a promising solution for monitoring deformations in the subsoil [91]. Displacements or deformations created in subsoil materials are transferred to a sensitive cable (sensor) through a trench or a borehole, causing changes in the light signal to be sent through the cable. By comparing the signals before and after deformation, it is possible to precisely determine the deformation amount of the surrounding materials. DSS systems are available on the market with a high measurement sensitivity of up to 0.5 $\mu\varepsilon$ [23]. Monitoring deformation by FO sensors has several advantages over conventional methods (conventional electrical strain gauge [92]), which are limited by the sensitivity to electromechanical interference and sensor corrosion.

DSS sensors have been used primarily for monitoring land subsidence and landslides [21, 22]. Liu et al. [25] adopted the DSS system in an in-situ experiment to monitor land subsidence in a borehole located in Tianjin (China). The authors have shown that DSS technology is effective for monitoring land subsidence in coastal areas. CEMENTYS (French company specializing in FO technology) have been using a DSS system (Brillouin-BOTDA (Optical Time Domain Analyzer)) for monitoring a buried pipeline with a length of 300 m in the French Alps since 2013. The area is subject to ground motion and CEMENTYS company is ensuring the pipeline integrity. To study strains on the pipeline body, three *Sensolux TM*® FO cables were glued directly on the surface of the pipeline. This 120° straight shape is needed to detect and measure strains in any flexural direction. This layout is also necessary to study its 3-dimensions behavior in time. The installed DSS system allows to follow the displacement and the stress in three dimensions (X, Y and Z) around the pipeline in real time and in the long term as presented in Fig. 9.4.

Recent studies have also used the DSS technology to improve the knowledge about hydrogeological processes occurring along the VZ (Table 9.5). Zhang et al. [93] used the DSS system to monitor micro-deformations associated with digging a new well in a rural area of the city of Mobara (Chiba, Japan). The FO cable was installed behind the PVC casing and cemented in two observation boreholes located at different distances from the new well (3 and 9 m). Small changes in deformation were observed in both boreholes while drilling the wells. The authors suggest that these changes were related to the hydrodynamic deformations (between fluid and solid) and the permeability variations of VZ materials. The injection of fluids into the VZ during

Table 9.4 An overview of recent applications of the DAS system for environmental monitoring

References	Measurements	DAS instrument	FO cable	Data collecting
[84]	Seismic monitoring Reservoirs imaging	DAS	SM FO cable (length: 977 m)	Gauge length: 10 m Spatial res.:1 m Duration of acquisitions: 4.5 days Frequency sampling: 1-kHz
[20]	Fracture monitoring in fractured Bedrock	iDAS (Silixa Ltd., UK)	Tight buffered cable 9/125 µm, SM fiber	Temporal sampling: 1 kHz Spatial sampling: 0.25 m
[64]	Soil/rock thermal properties (boreholes installation)	DAS A1-R (FEBUS, Fr)	SM FO cable: BRUsens DAS 6.0 mm non-metallic, from Solifos—Switzerland	Installation/Calibration
[87]	Monitoring of groundwater flow Ambient seismic noise measurements	iDAS (Silixa Ltd., UK)	SM FO cable of 1280 m length	Gauge length: 10 m Spatial res.: 0.25–1.0 m Frequency sampling: 5–50 kHz
[88]	Surface imaging using ambient noise	iDAS (Silixa Ltd., UK)	SM telecommunication fibers	Gauge length: 10 m Spatial res.: 2 m Frequency sampling: 500 Hz Generated data: 8 TB
[19]	Fracture detection and imaging through relative seismic velocity changes using DAS and ambient seismic noise	iDAS (Silixa Ltd., UK)	Tactical SM	Gauge length: 10 m Duration of acquisitions: 13 h Frequency sampling: 30 s
[89]	Seismic monitoring of the near surface	iDAS (Silixa Ltd., UK)	Comparison of 4 cables: (1) a gel-filled polyethylene cable; (2) a tight-buffered, tactical cable; (3) a gel-filled, steel-armored cable; (4) a tight-buffered, steel-tubing cable	Gauge length: 10 m Duration of acquisitions: 3 weeks Spatial res.:1 m Frequency sampling: 1-kHz Generated data: 2.7 TB
[90]	Seismic monitoring Geophone and DAS comparison VSP data acquisition	DAS	SM FO cable	Gauge length: 10 m Spatial resolution: 1.0 m
[87]	Geophone and DAS system comparison VSP data acquisition	iDAS (Silixa Ltd., UK)	SM FO cable	Gauge length: 10 m Spatial resolution: 2.0 m
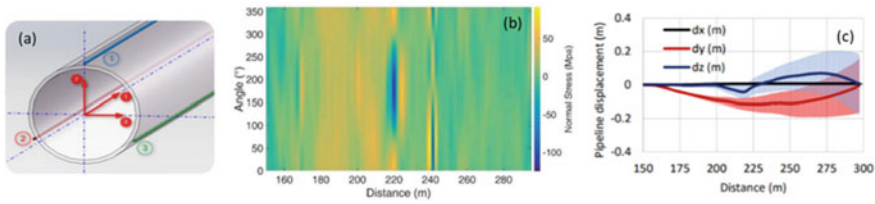
Fig. 9.4 **a** The disposition of FO (sensors) on the surface of the pipeline, **b** the stress and **c** displacement variations in three dimensions (X, Y and Z) observed around the pipeline

drilling causes changes in fluid pressure, and can induce change in the properties of the VZ geological facies (mainly in heterogeneous and permeable materials). A similar study was carried out by Lei et al. [24] in the same city, during a pumping experiment. A vertical well located between two pumping wells was equipped with a DSS cable sensitive to micro-deformation down to a depth of 300 m. The results obtained showed that compressive deformation was observed in the VZ materials after several hours of pumping. The authors also underlined the direct link between the observed deformations and the properties (permeability, heterogeneity) of the VZ materials. The highest deformations were observed in the more permeable and heterogeneous layers (sandy sediments) during the pumping period. In a laboratory study, Zhang et al. [23] observed deformations (dilatation) using a DSS system on a sample of sandstone rock (high clay content and low permeability) during its saturation processes. The authors suggested that this deformation is related to two factors: (i) the change in pore pressure due to the accumulation of water in the pores of the sample; (ii) and the swelling effect of the clay. This works has highlighted that the DSS system not only has the potential to provide geomechanical information on the VZ materials, which can play an important role in preventing landslide hazards and land subsidence, but can also give valuable information on the link between the deformation of materials and the fluids flow in the VZ. This set of findings improve our understanding of the role of fluid flow in rock deformation within the VZ.

9.2.4   Chalcogenide FO Sensors

Fiber Evanescent Wave Spectroscopy (FEWS) simply requires dipping the fiber into a liquid under analysis or putting it in direct contact with the analyte. FEWS using chalcogenide glass fibers is an efficient tool land. The chalcogenide fibers can be specifically shaped for head sensing thanks to the fibers' thermo-forming capability [94]. It also allows investigation in different fields; e.g. the detection of contaminants in waste water [16, 95], the monitoring of chemical or industrial processes [96, 97], the detection of bacterial contamination in food [98, 99], and applications in the medical field [100]. Consequently, these materials can contribute to the development

**Table 9.5** Examples of recent applications of the DSS system for environmental monitoring

References	Measurements	DSS instrument	FO cable	Data collecting
[21]	Measurements of distributed deformations related to water pumping in an aquifer in Shengze, southern Yangtze Delta, China	Advantest N8511 BOTDR analyzer (Tokyo, Japan)	Tight-buffed strain cables, 2 mm diameter (Nanzee Sensing, Suzhou, China) FO cable installed in a vertical borehole 150 m deep	Spatial res.: 1 m Noise level of 40 $\mu\varepsilon$ Duration of acquisitions: from 2014 to 2016
[23]	Measure rock deformation while injecting water into low-permeability dry sandstone. Laboratory study	(NBX-7020; Neubrex Co., Ltd., Kobe, Japan) Maximum measurement range of 20 km	Strain FO cable, the FO cable was wound helically around the rock sample	Measurement accuracy: 0.5 $\mu\varepsilon$ Spatial res.: 2 cm Material: sandstone sample (from Gunma, Japan)
[24]	Geomechanical monitoring Distributed strain measurements at a pumping test (Mobara, Japan)	Neubrescope NBX-8000 device	A strain FO cable was custom-made for this study FO cable was installed behind the PVC casing in an observation well located between three pumping wells	Spatial res.: 1 cm Temporal res.: 5 min
[25]	Land subsidence monitoring in Tianjin, China	AV6419 optical fiber temperature/strain analyzer produced by the 41st Research Institute of China Electronics Technology Group Corporation, China	FO cable 2 mm diameter produced by Suzhou NanZee Sensing Ltd., China FO cable installed in a vertical borehole 100 m deep	Spatial res.: 1 m Resolution accuracy: 10 cm Strain measurement accuracy is ± 50 $\mu\varepsilon$
[93]	Strain monitoring in two observations wells (where FO cables were installed) while drilling a new well. Mobara city (Chiba, Japan)	NBX-SR7000 (Neubrex Co., Ltd., Japan) Maximum measurement range of 25 km	Stainless-steel wire reinforced cable (strain cable with rectangular shape, 2.0×3.8 mm) FO cable installed behind the PVC casing in tow observations wells 144 m deep	Measurement accuracy: 0.5 $\mu\varepsilon$ Spatial res.: 5 cm

of pioneering glass technologies in IR spectral windows to design innovative optical sensors [101].

An optical sensor based on mid-IR fluorescence to probe gas molecules has already been developed using a transmission configuration instead of FEWS for the detection of carbon dioxide by means of the 4.3 μm emission of a Dy^{3+} doped chalcogenide fiber [37]. Due to their high degree of mechanical integration and reliability (connectors, fiber coating techniques), optical fiber-based sensors are designed for commercial purposes. Compared to FEWS using undoped chalcogenide fibers as the sensitive media, this sensor has been developed in order to produce its own mid-IR fluorescence source. The resolution of real time detection could be enhanced and the overall compactness and complexity of the optical system can be efficiently reduced. FEWS relies on the optical absorption of the surrounding environment of the optical fiber, with a typical penetration depth of a few micrometers for the evanescent waves. The degree of integration of such devices is potentially high thanks to the rare earth doped chalcogenide fiber converting the pump signal from a visible or near infrared laser diode to mid-IR. By means of frequency conversion, the sensor could allow remote monitoring using silica fibers considering that the inverse photon conversion from mid-IR to visible or near-IR can be used based on a rare earth up-conversion phenomenon [101]. An all-optical IR fiber sensor for in-situ carbon dioxide monitoring was developed by BRGM, University of Caen, University of Rennes and IDIL [38]. This sensor can be typically deployed over the kilometer range with a sensitivity of few hundreds of ppm, making it suitable for field operations. The sensors prototypes were tested in a 100 m deep dry pit at the LSBB facility (Low-Noise Underground Laboratory) in Rustrel, France (Fig. 9.5).

The results led to the development of a carbon dioxide prototype for field experiments comprising a Dy^{3+}: GaGeSbS MWIR emitting fiber and an Er^{3+}: GaGeSbS conversion fiber. Carbon dioxide sensing experiments were performed using this all-optical sensor for various CO_2 concentrations ranging from 0.2% (2000 ppm) to 100% [38].

The All-optical CO_2 detection system present key advantages over electronic devices, especially for high pressure working conditions and electromagnetic compatibilities, since there are no electronic parts within an all-optical CO_2 detection head. The originality of this approach lies in the development of an all-optical method allowing real time in-situ analysis combined with a remote, direct and continuous monitoring in a wide range of concentrations.
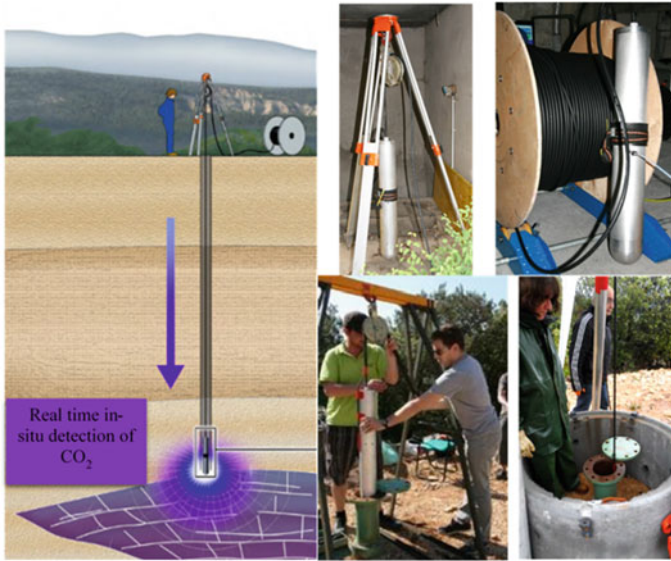
Fig. 9.5 All-optical IR FO sensor deployed in an experimental site located in Rustrel, France (Low-Noise Underground Laboratory (LSBB))

9.3   O-ZNS Project: Main Objectives, First Results and Instrumentation Strategy

9.3.1   The Beauce Limestone Aquifer

The Beauce limestone aquifer is located in the Centre-Val de Loire Region (France) and extends over 9700 km^2 [102] between the Seine river (northeastern part) and the Loire river (southwestern part). This mostly unconfined aquifer constitutes one of the largest groundwater reservoirs in France with an average stock of water of 20 billion m^3 [103], and is mainly composed of Cenozoic limestone from upper Oligocene to lower Miocene whose origin is mostly lacustrine [104]. The thickness and the topography of the Beauce limestone aquifer ranges from 10 to 200 m and from 70 m up to 190 m [105]. The Beauce represents the main cereal-producing region in Europe [106] and its land use consists essentially in agriculture (74%), 50% of which is irrigated [107]. Over the past decades, this intensive agricultural activity have led to the implementation of governmental policies and regulatory measures whose actions aim at controlling water withdrawals [108, 109] and preserving groundwater quality, particularly towards pesticides and nitrates contaminations [110, 111].

9.3.2 The Objectives of the O-ZNS Project

The VZ, which is identified as a key component of the Critical Zone (CZ), represents a cornerstone in assessing water balance, understanding groundwater recharge and managing contamination problems for the protection of groundwater resources. To this aim, a growing body of studies focused on deciphering the complex and coupled physical, geochemical, and microbiological processes which govern the mass and heat transfers within the VZ [2, 112].

In this context, the main target of the O-ZNS is to acquire original and unique long-term data on the reactive transfer processes of mass and heat in the VZ. The project aims to follow in-situ and in real time the highly coupled physical, chemical, and biological processes that might influence the water flow and solutes transport in the VZ. The O-ZNS project also aims at assessing the performance of all types of instrumentation dedicated to non-destructive measurements or local sampling of fluids, geological facies, and microbial communities in the VZ.

The O-ZNS experimental site is under development in an agricultural field located in the heart of the Beauce Region, at Villamblain, about 30 km northwest of Orléans (DMS coordinates: X = 48° 1′ 5.131″; Y = 1° 34′ 55.333″) (Fig. 9.6). It consists of the installation of an exceptional access well (diameter ~4 m and depth ~20 m) surrounded by several boreholes. This allows the instrumentation of the entire VZ column, from the soil surface down to the aquifer (saturated zone fluctuating between −15 and −23 m deep).
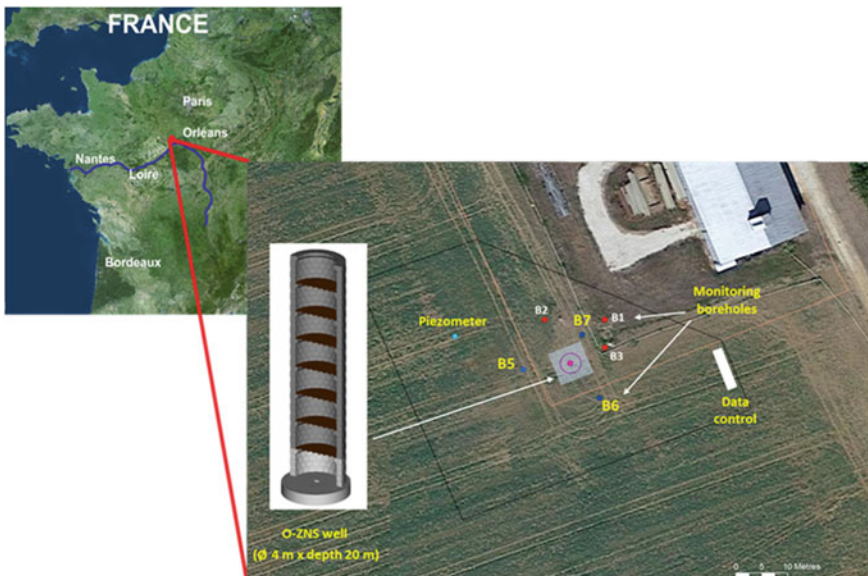
Fig. 9.6 O-ZNS experimental site located in Villamblain (30 km northwest of Orléans, France) at the heart of the Beauce Region
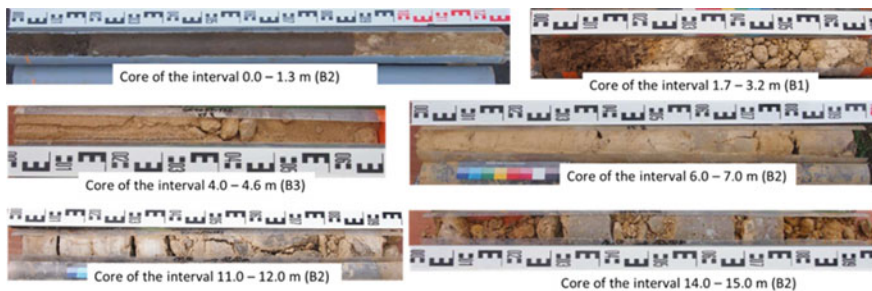
9.3.3 Preliminary Investigations Made Within the Framework of O-ZNS Project

The first geotechnical investigations were made at the O-ZNS experimental site in the spring of 2017.Three cored boreholes (B1, B2, B3, cf. Fig. 9.7) have been drilled on March 2017 from 0 to 20 m deep. The description made by visual examination of undisturbed cores showed that the VZ profile presents both high vertical and lateral lithological heterogeneities [113, 114].

Three main lithological units were identified along the VZ profiles from the soil surface down to 20 m deep (Fig. 9.7):

- 0.0–1.5 m: silt loam soil typical of the Beauce region and referred to as a Hypereutric Cambisol according the World Reference Base for Soils [115],
- 1.5–8.0 m: fragmented powdery limestone facies that was cryoturbated in its upper part and which also contains calcareous sand interbeds,
- 8.0–20 m: massive, fractured or altered/karstified hard limestone rock.

Many authors stressed that the determination of the hydraulic properties, i.e. water retention and hydraulic conductivity, of the VZ materials is critical for a precise assessment of water flow, and mass and heat transfers from the soil surface down to the aquifer [116–120]. The first study conducted within the framework of the O-ZNS project was dedicated to the determination of hydraulic properties of soft and hard representative samples selected along the whole VZ profile and taken from three cored boreholes drilled in spring 2017 (B1, B2, B3 on Fig. 9.6). The hydraulic properties of the samples were determined in the ISTO vadose zone laboratory using the multistep outflow method applied by a triaxial system and related to physical, mineralogical and chemical analysis made on the same samples in order to investigate water flow pathways [113, 114]. The results of this work highlighted the high heterogeneity of the properties of both soft and hard VZ materials and provided valuable information on the influence of the presence or absence of different types of secondary minerals and the impact of alteration processes on water flow within the VZ.

Core of the interval 0.0 – 1.3 m (B2)

Core of the interval 1.7 – 3.2 m (B1)

Core of the interval 4.0 – 4.6 m (B3)

Core of the interval 6.0 – 7.0 m (B2)

Core of the interval 11.0 – 12.0 m (B2)

Core of the interval 14.0 – 15.0 m (B2)

Fig. 9.7 Lithological description of the materials encountered throughout the VZ column of the O-ZNS experimental site

Based on these laboratory hydraulic properties measurements, a second on-going study is focused on the simulation of water flow and the estimation of water travel time through the VZ performed by a virtual tracing experiment simulated over a period of more than 50 years using HYDRUS-1D software [121] and meteorological and water table level data as input. The primary results showed a mean water travel time of 18.7 and 29.0 years for the initial (1 mg/L) and the peak concentration of bromide to reach the maximum water table level (-14.84 m), respectively [114, 122]. The variability in the water travel time within the VZ was mainly induced by two key factors: the meteorological data and the high heterogeneity in the properties of the VZ materials, especially through the weak permeability of the massive limestone rock facies which could lead to the occurrence of perched water tables in the VZ profile.

9.3.4 Instrumentation Strategy of the O-ZNS Project

The O-ZNS project aims to monitoring the mass and heat transfer processes within the VZ of the Beauce aquifer. This broad objective will be addressed thanks to the instrumentation of (i) the vadose zone laboratory based in Orléans (ISTO); (ii) the large VZ access well that will be drilled in 2021; (iii) the surrounding boreholes, including those drilled in 2017 and 2020, three of which are currently instrumented with FO cables (Sect. 9.4). The results obtained through the first multidisciplinary studies made within the framework of the O-ZNS project focused on properties obtained at the laboratory scale and within the matrix component of the VZ of the Beauce limestone aquifer. However, optical imaging made on the boreholes and lithological description made on the core samples [113, 122] showed that natural (macro-) fractures with possible karstification were observed at the field scale and have been episodically subjected to intense leaching of water under or close to fully saturated conditions. The water flow and solute transport observed at the field scale could consequently be significantly faster and influenced by preferential flow paths through interconnected fracture networks, notably after exceptional heavy rainfall [123, 124].

The identification and characterization of these open fractures networks and the understanding of the location of these preferential flow pathways is thus essential. This represents one of the key objectives of the O-ZNS project towards deciphering the complex processes which govern the mass and heat transfers within this highly heterogeneous VZ. To this end, a wide variety of environmental monitoring solutions are actually being explored using coupled geological, hydrogeological and geophysical monitoring techniques for the in-situ monitoring of water flow and solute transport within the whole VZ column and some of the key compartments of the CZ (rhizosphere-soil-VZ-aquifer) (Fig. 9.8). This includes, inter alia, hydrogeological monitoring solutions, some of which are considered innovative [125–132].

A second objective of the O-ZNS project is to support the development of innovative methods and sensors (geophysical imagery, microchips, coupling between
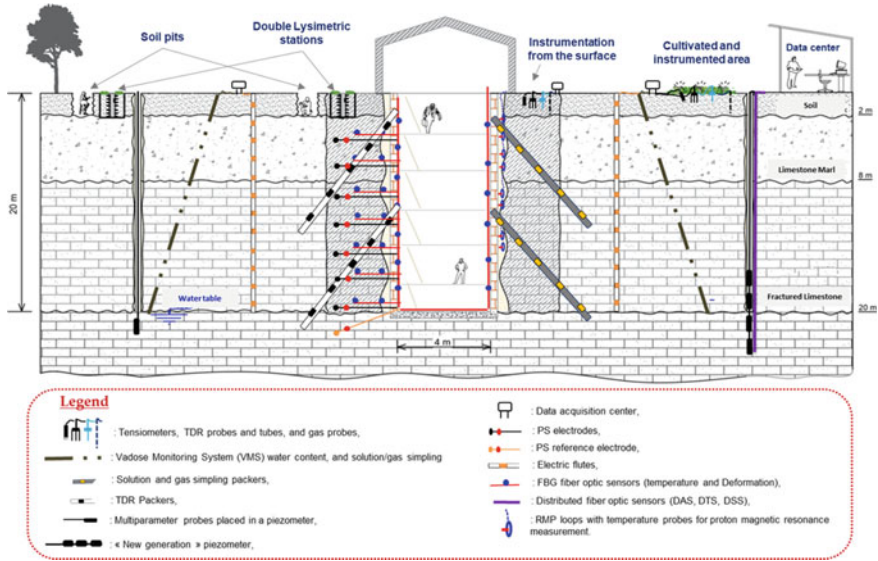
Fig. 9.8 Schematic sketch representing the spatial deployment of the environmental monitoring instrumentations at the O-ZNS observatory site (Villamblain, Orléans, France)

knowledge of "disciplines" and joint interpretations, etc.) for a fine characterization of the dynamics of the VZ. Among these methods is the FO technology, which is increasingly used for environmental monitoring applications.

9.4 Installation of FO Sensors on the O-ZNS Experimental Site

As part of O-ZNS instrumentation, three types of distributed FO sensors (flexible sensing cables cf. Table 9.6) were installed in a continuous loop along three boreholes (with a depth varying from 21 to 23 m) surrounding the future large observatory well and were connected to a data center (Fig. 9.9a). These sensors will allow the monitoring of fluid flow, the characterization of rock fractures, and the micro-movements detection in the VZ of the Beauce limestone aquifer. The FO cables were supplied by the Solifos company (Switzerland) and installed by the CEMENTYS company (France) in July 2020. The disposal of the cables is shown in Fig. 9.9. As these cables are flexible, they were installed in a continuous loop along boreholes (B5, B6, B7) without splicing. The ends of the cables are located inside the data control. They will soon be connected with the interrogators respectively to each technology.

Table 9.6 summarizes the main characteristics of the three cables used. Considering that the DTS cable consists of four MM fibers (two 50 μm and two 62.5 μm), the DSS and DAS cables are made up of one and four SM fibers, respectively.

Table 9.6 Main characteristics of FO cables installed on the O-ZNS experimental site

Characteristics	DTS cable	DAS cable	DSS cable
Color	Black	Green	Blue
Diameter (mm)	4.0	6.5	2.8
Cable type	Loose	Loose	Tight
FO	2 MM-FO (62.5/125)	4 SM-FO	1 SM-FO
Sensitivity	Temperature	Acoustic noise/Temperature	Strain/Deformation
Interrogation system	Raman	Rayleigh	Brillouin, FBG
Other information	Non-metallic cable, compact design, flexibility	Non-metallic cable, good acoustic response, high tensile strength high chemical resistance	Non-metallic cable, protective and stress transfer layer, strain range up to 1% (10,000 μ strain)
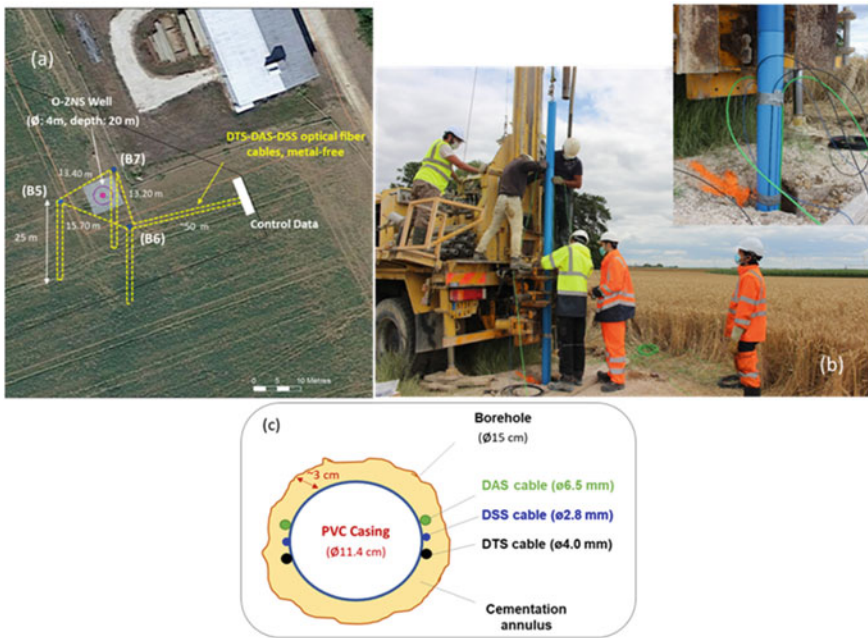
Fig. 9.9 **a** Aerial photography of the O-ZNS experimental site showing the position of the main well and the three surrounding monitoring boreholes (B5, B6, B7). The FO cables were installed in loops covering the three boreholes (drawn in yellow). **b** The installation of FO cables (DTS: black, DAS: green, DSS: blue) in the three boreholes made with CEMENTYS in July 2020. **c** Axial cross section of the borehole showing the area behind casing installation of FO cables

These cables were chosen based on their flexibilities, their resistances in a harsh environment and their compositions. To avoid any disruption of future geophysical measurements on the O-ZNS site, the cables were installed in the boreholes without metal reinforcements or protections. Illustrations of the installation are shown in Fig. 9.9. The cables were installed behind the PVC casing and sealing with a mixture of 60% of sand (0/4 mm), 40% of limestone filler and 20% of water to ensure a good coupling between the FO cables and the materials of the VZ. The use of cement was indeed excluded because of the geochemical perturbations (pH) induced by the reaction between cement and the limestone rocks of the VZ.

After their installation in the boreholes, all fibers were checked with an OTDR (Optical Time Domain Reflectometer). The purpose of the OTDR measurements was to verify that the fibers have not been damaged during the installation operations along the boreholes. It is a method which makes it possible to characterize the FO from only one of its ends, and leads to the precise localization of the faults, to the measurement of the attenuation of the fiber and to the differential losses between two chosen points of the fiber. Thanks to the OTDR measurements we have confirmed that the FO installed on the O-ZNS site are intact and present no faults over its entire linear.

The multi FO sensors system installed at the O-ZNS site will help in the fine characterization of the subsoil structure in the near O-ZNS well zone through the three boreholes B5, B6 and B7. The DTS system will provide continuous and real-time temperature profile information at resolutions up to 0.01 °C with a spatial resolution down to centimeter scale. This information will be very useful for the identification of active fractures in the VZ of the O-ZNS site under ambient flow conditions or following a rapid heating episode (using heat as a tracer for fracture detection [9, 80]). The DTS will also be used to monitor heat movements throughout the depth of the VZ to estimate the flow rates of fluids in boreholes [68, 70]. Monitoring of the natural fluid flow system in the VZ is important for accurate predictions of the fate and transfer of contaminants. The DSS systems will be used for the monitoring of consolidation and geomechanical deformations of VZ materials with a high sensitivity. Recent studies have shown that it can also be used to understand the deformations (or micro-deformations) associated with the fluids flow in the VZ through hydromechanical coupling [23]. In our case, the DSS system will be very useful for the detection of micro-movements linked to the digging of the O-ZNS well, to fluid infiltration and to measure the deformations in the capillary fringe area linked to the recharge/discharge of the aquifer. DAS technology also shows promise for the detection and monitoring of cracks and fractures throughout the VZ [19]. The use of this technology for the O-ZNS project will provide key information on the characteristics and geometry of fractures by monitoring changes in seismic velocity. However, this technology is, to date, at an early stage of maturity and it is necessary to characterize their degree of complementarity/coupling with traditional seismic measurements. Comparative seismic measurements (DAS and conventional seismic methods) on the surface and in boreholes are planned in the O-ZNS site to assess the potential of this technology in environmental monitoring. Detailed research is also needed to study the sensitivity of DAS measurements to variations in environmental factors (temperature, pH, Eh,

micro-movements, etc.). The information which will be re-purified (or confirmed) by this multi-sensors FO device will constitute an interoperable database which can improve the understanding of coupled and complex processes governing water flow and solute (including contaminants) and heat transfers in the VZ of the Beauce limestone aquifer.

9.5 Conclusion

This chapter provides a comprehensive overview of fiber optic sensors (distributed and point sensors) and contains numerous results and references from recent scientific publications and industrial technical papers on the principles, types and recent environmental monitoring applications of FO sensors. The deployment of distributed fiber optic sensors at the O-ZNS site was also presented. Thanks to their intrinsic characteristics and flexibility, fiber optic sensors are increasingly used in environmental monitoring applications, especially for monitoring the vadose zone. They are insensitive to electromagnetic fields and can provide information in real time and continuously over several kilometers (in the case of distributed sensors). However, there are still some limitations that prevent the generalization of this technology in monitoring designs. The high cost of interrogators remains the major constraint hindering the adoption of fiber optic systems in environmental monitoring applications. Many technological innovations have been made in recent years to improve the performance of interrogator systems and increase their value for money. Further improvements are still needed to further reduce costs and make them more affordable. For a successful installation, good coupling between the sensors and the materials (or the structure to be monitored) is also essential. The installation of the sensors and the cementing operations must be carried out with sufficient care to ensure good sensor-material contact and to avoid the development of a vacuum which disturbs the measurements. Improvements in spatial resolution and measurement range are also required to make it a promising method in environmental applications. Additional in-situ studies, including comparisons with results obtained with traditional sensors, are also essential to validate the prototypes under development for monitoring physicochemical parameters (pH, Eh, salinity, metal ions, etc.) and gases concentrations. The multi-FO sensor system (DTS, DSS and DAS) which were successfully installed at the O-ZNS site will help characterize the temperature, deformations and micro-movements near the O-ZNS main well and will improve our understanding of mass and heat transfers within the highly heterogeneous VZ of the Beauce aquifer.

References

1. Nimmo JR (2005) Unsaturated zone flow processes. In: Anderson MG, Bear J (eds) Encyclopedia of hydrological sciences. Wiley, Chichester, pp 2299–2322
2. Arora B, Dwivedi D, Faybishenko B, Jana RB, Wainwright HM (2019) Understanding and predicting vadose zone processes. Rev Mineral Geochem 85(1):303–328
3. Stephens DB (2018) Vadose zone hydrology. CRC Press
4. Philippe É, Habets F, Ledoux E, Goblet P, Viennot P, Mary B (2011) Improvement of the solute transfer in a conceptual unsaturated zone scheme: a case study of the Seine River basin. Hydrol Process 25(5):752–765
5. Grattan KT, Meggitt BT (eds) (1995) Optical fiber sensor technology, vol 1. Chapman & Hall, London
6. Or D, Tuller M, Stothoff S (2006) Review of vadose zone measurement and monitoring tools for Yucca Mountain performance confirmation program. US Nuclear Regulatory Commission report under contract NRC-02-02-012
7. Jin G, Roy B (2017) Hydraulic-fracture geometry characterization using low-frequency DAS signal. Lead Edge 36(12):975–980. https://doi.org/10.1190/tle36120975.1
8. Mellors RJ, Messerly M, Morris J, Ryerson R, Sherman C, Yu C, Allen G (2018) Modeling potential EGS signals from a distributed fiber optic sensor deployed in a borehole (No. LLNL-PROC-745469). Lawrence Livermore National Lab. (LLNL), Livermore, CA, United States
9. Read T, Bour O, Bense V, Le Borgne T, Goderniaux P, Klepikova MV et al (2013) Characterizing groundwater flow and heat transport in fractured rock using fiber-optic distributed temperature sensing. Geophys Res Lett 40(10):2055–2059
10. Read T, Bour O, Selker JS, Bense VF, Le Borgne T, Hochreutener R, Lavenant N (2014) Active-distributed temperature sensing to continuously quantify vertical flow in boreholes. Water Resour Res 50(5):3706–3713
11. Gambolati G, Teatini P (2015) Geomechanics of subsurface water withdrawal and injection. Water Resour Res 51:3922–3955
12. Huang AB, Wang CC, Lee JT, Ho YT (2016) Applications of FBG-based sensors to ground stability monitoring. J Rock Mech Geotech Eng 2016(8):513–520
13. Weiss JD (2003) U.S. patent no. 6,581,445. U.S. Patent and Trademark, Washington, DC
14. Sayde C, Gregory C, Gil-Rodriguez M, Tufillaro N, Tyler S, van de Giesen N, English M, Cuenca R, Selker JS (2010) Feasibility of soil moisture monitoring with heated fiber optics. Water Resour Res 46:W06201. https://doi.org/10.1029/2009WR007846
15. Ciocca F, Lunati I, Van de Giesen N, Parlange MB (2012) Heated optical fiber for distributed soil-moisture measurements: a lysimeter experiment. Vadose Zone J
16. Michel K, Bureau B, Boussard-Plédel C, Jouan T, Adam JL, Staubmann K, Baumann T (2004) Monitoring of pollutant in waste water by infrared spectroscopy using chalcogenide glass optical fibers. Sens Actuators B Chem 101(1–2):252–259. https://doi.org/10.1016/j.snb.2004.03.014
17. Michel K, Bureau B, Boussard-Pledel C, Adam J-L (2015) Réalisation d'un capteur à fibre optique infrarouge pour la détection des polluants dans les eaux usées. Déchets sciences et techniques [En ligne], N°34, mis à jour le: 04/03/2015. http://lodel.irevues.inist.fr/dechets-sciences-techniques/index.php?id=2102. https://doi.org/10.4267/dechets-sciences-techniques.2012

18. Parker T, Shatalin S, Farhadiroushan M (2014) Distributed acoustic sensing—a new tool for seismic applications. First Break 32(2):61–69. https://doi.org/10.3997/1365-2397.2013034

19. James SR, Knox HA, Preston L, Knox JM, Grubelich MC, King DK et al (2017) Fracture detection and imaging through relative seismic velocity changes using distributed acoustic sensing and ambient seismic noise. Lead Edge 36(12):1009–1017

20. Becker MW, Coleman TI, Ciervo CC (2020) Distributed acoustic sensing (DAS) as a distributed hydraulic sensor in fractured bedrock. Water Resour Res. e2020WR028140

21. Zhang C, Shi B, Gu K, Liu S, Wu J, Zhang S, Zhang L, Jiang H, Wei G (2018) Vertically distributed sensing of deformation using fiber optic sensing. Geophys Res Lett 45(21):11–732

22. Murdoch LC, Germanovich LN, DeWolf SJ, Moysey SMJ, Hanna AC, Kim S, Duncan RG (2020) Feasibility of using in situ deformation to monitor CO_2 storage. Int J Greenhouse Gas Control 93:102853. https://doi.org/10.1016/j.ijggc.2019.102853

23. Zhang Y, Xue Z (2019) Deformation-based monitoring of water migration in rocks using distributed fiber optic strain sensing: a laboratory study. Water Resour Res 55(11):8368–8383

24. Lei X, Xue Z, Hashimoto T (2019) Fiber optic sensing for geomechanical monitoring:(2)-distributed strain measurements at a pumping test and geomechanical modeling of deformation of reservoir rocks. Appl Sci 9(3):417

25. Liu SP, Shi B, Gu K, Zhang CC, Yang JL, Zhang S, Yang P (2020) Land subsidence monitoring in sinking coastal areas using distributed fiber optic sensing: a case study. Nat Hazards 103(3):3043–3061

26. Lu P, Lalam N, Badar M, Liu B, Chorpening BT, Buric MP, Ohodnicki PR (2019) Distributed optical fiber sensing: review and perspective. Appl Phys Rev 6(4):041302

27. Zhicheng Z, Liu K, Han X, Lin J (2019) Review of fiber-optic distributed acoustic sensing technology. Instrumentation 6(4)

28. Wen H, Peng Z, Jian J, Wang M, Liu H, Mao ZH et al (2018) Artificial intelligent pattern recognition for optical fiber distributed acoustic sensing systems based on phase-OTDR. In: 2018 Asia communications and photonics conference (ACP). IEEE, pp 1–4

29. Wang X, Lee J, Thigpen B, Vachon GP, Poland SH, Norton D (2008) Modeling flow profile using distributed temperature sensor (DTS) system. In: Intelligent energy conference and exhibition. Society of Petroleum Engineers

30. Sherman C, Mellors R, Morris J, Ryerson F (2019) Geomechanical modeling of distributed fiber-optic sensor measurements. Interpretation 7(1):SA21–SA27

31. Janting J, Pedersen JK, Woyessa G, Nielsen K, Bang O (2019) Small and robust all-polymer fiber Bragg grating based pH sensor. J Lightwave Technol 37(18):4480–4486

32. Kishore PVN, Madhuvarasu SS, Putha K, Moru S, Gobi KV (2016) Hydrogel coated fiber Bragg grating based chromium sensor. In: Optical sensing and detection IV, vol 9899. International Society for Optics and Photonics, p 98991B

33. Guzman-Sepulveda JR, Ruiz-Perez VI, Torres-Cisneros M, Sanchez-Mondragon JJ, May-Arrioja DA (2013) Fiber optic sensor for high-sensitivity salinity measurement. IEEE Photonics Technol Lett 25(23):2323–2326

34. Yeo TL, Sun T, Grattan KT, Parry D, Lade R, Powell BD (2005) Polymer-coated fiber Bragg grating for relative humidity sensing. IEEE Sens J 5(5):1082–1089

35. Elsherif M, Moreddu R, Hassan MU, Yetisen AK, Butt H (2019) Real-time optical fiber sensors based on light diffusing microlens arrays. Lab Chip 19(12):2060–2070

36. Delepine-Lesoille S, Bertrand J, Lablonde L, Phéron X (2012) Distributed hydrogen sensing with Brillouin scattering in optical fibers. Photonics Technol Lett 24(17)

37. Starecki F, Charpentier F, Doualan JL, Quetel L, Michel K, Chahal R et al (2015) Mid-IR optical sensor for CO_2 detection based on fluorescence absorbance of Dy^{3+}: $Ga_5Ge_{20}Sb_{10}S_{65}$ fibers. Sens Actuators B Chem 207:518–525

38. Starecki F, Braud A, Doualan J-L, Ari J, Boussard-Plédel C, Michel K, Nazabal V, Camy P (2019) All-optical carbon dioxide remote sensing using rare earth doped chalcogenide fibers. Opt Lasers Eng 122:328–334. https://doi.org/10.1016/j.optlaseng.2019.06.018

39. Barrias A, Casas JR, Villalba S (2016) A review of distributed optical fiber sensors for civil engineering applications. Sensors 16(5):748

40. Hartog A (2017) An introduction to distributed optical fibre sensors. CRC Press, 442pp
41. Schenato L (2017) A review of distributed fibre optic sensors for geo-hydrological applications. Appl Sci 7(9):896. https://doi.org/10.3390/app7090896
42. Di Sante R (2015) Fibre optic sensors for structural health monitoring of aircraft composite structures. Recent advances and applications. Sensors 15(8):18666–8713
43. Annamdas KKK, Annamdas VGM (2010) Review on developments in fiber optical sensors and applications. In: Fiber optic sensors and applications VII, vol 7677. International Society for Optics and Photonics, p 76770R
44. Mihailov SJ (2012) Fiber Bragg grating sensors for harsh environments. Sensors 12(2):1898–1918
45. Miah K, Potter DK (2017) A review of hybrid fiber-optic distributed simultaneous vibration and temperature sensing technology and its geophysical applications. Sensors 17(11):2511
46. Bao Y, Huang Y, Hoehler MS, Chen G (2019) Review of fiber optic sensors for structural fire engineering. Sensors 19(4):877
47. Ferraro P, de Natale G (2002) On the possible use of optical fiber Bragg gratings as strain sensors for geodynamical monitoring. Opt Laser Eng 37:115–130
48. Lecoy P (2016) Les fibres optiques en capteurs et en instrumentation. La Revue 3 E. I 85
49. Hill K, Meltz G (1997) Fiber Bragg grating technology fundamentals and overview. J Lightwave Technol 15(8):1263–1276
50. Kashyap R (2009) Fiber Bragg gratings. Academic Press, Cambridge
51. Drusová S, Wagterveld RM, Wexler AD, Offerhaus HL (2019) Dynamic consolidation measurements in a well field using fiber Bragg grating sensors. Sensors 19(20):4403
52. Alemohammad H, Azhari A, Liang R (2017) Fiber optic sensors for distributed monitoring of soil and groundwater during in-situ thermal remediation. In: Fiber optic sensors and applications XIV, vol 10208. International Society for Optics and Photonics, p 102080I
53. Wang J, Jiang L, Sun Z, Hu B, Zhang F, Song G, et al (2017) Research on the surface subsidence monitoring technology based on fiber Bragg grating sensing. Photonic Sens 7(1):20–26
54. Cong J, Zhang X, Chen K, Xu J (2002) Fiber optic Bragg grating sensor based on hydrogels for measuring salinity. Sens Actuators B Chem 87(3):487–490
55. Aleixandrea M, Correderab P, Hernanzb ML, Sayago I, Horrillo MC, Gutierrez-Monreal J (2007) Study of a palladium coated Bragg grating sensor to detect and measure low hydrogen concentrations. In: Proceedings of the 2007 Spanish conference on electron devices, 31 Jan–2 Feb 2007, Madrid, Spain, pp 223–225
56. Selker JS et al (2006) Distributed fiber-optic temperature sensing for hydrologic systems. Water Resour Res 42
57. Tyler SW, Selker JS, Hausner MB (2009) Environmental temperature sensing using Raman spectra DTS fiber-optic methods. Water Resour Res 45(4)
58. Baldwin CS (2014) Brief history of fiber optic sensing in the oil field industry. In: Fiber optic sensors and applications XI, vol 9098. International Society for Optics and Photonics, p 909803
59. Koudelka P, Petrujova B, Latal J, Hanacek F, Siska P, Skapa J, Vasinek V (2010) Optical fiber distributed sensing system applied in cement concrete commixture research. Radio Eng 19(1):172–177
60. Brown G (2008) Downhole temperatures from optical fiber. Oilfield Rev 20(4):34–39
61. Molenaar MM, Hill D, Webster P, Fidan E, Birch B (2012) First downhole application of distributed acoustic sensing for hydraulic-fracturing monitoring and diagnostics. SPE Drill Completion 27(01):32–38. https://doi.org/10.2118/140561-PA
62. Daley TM, Freifeld BM, Ajo-Franklin J, Dou S, Pevzner R, Shulakova V, Kashikar S, Miller DE, Goetz J, Henninges J, Lueth S (2013) Field testing of fiber-optic distributed acoustic sensing (DAS) for subsurface seismic monitoring. Lead Edge 32(6):699–706. https://doi.org/10.1190/tle32060699.1
63. Kasahara J, Hasada Y, Kuzume H, Fujise Y, Yamaguchi T (2019) Seismic feasibility study to identify supercritical geothermal reservoirs in a geothermal borehole using DTS and DAS. In: 81st EAGE conference and exhibition 2019, vol 2019, no 1. European Association of Geoscientists & Engineers, pp 1–5

64. Ringstad C, Røed MH, Jestin C, Calbris G, Eliasson P, Jordan M, Wüstefeld A (2020) A multi-fibre optic sensing system for cross-well monitoring at the Svelvik CO_2 field lab. In: First EAGE workshop on fibre optic sensing, vol 2020, no 1. European Association of Geoscientists & Engineers, pp 1–5

65. Selker J, Van de Giesen N, Westhoff M, Luxemburg W, Parlange MB (2006) Fiber optics opens window on stream dynamics. Geophys Res Lett 33(24):24401. https://doi.org/10.1029/2006GL027979

66. Westhoff MC, Savenije HHG, Luxemburg WJ, Stelling GS, Van de Giesen NC, Selker JS et al (2007) A distributed stream temperature model using high resolution temperature observations. Hydrol Earth Syst Sci 11(4):1469–1480

67. Keller CA, Huwald H, Vollmer MK, Wenger A, Hill M, Parlange MB, Reimann S (2011) Fiber optic distributed temperature sensing for the determination of the nocturnal atmospheric boundary layer height. Atmos Meas Tech 143–149

68. Freifeld BM, Finsterle S, Onstott TC, Toole P, Pratt LM (2008) Ground surface temperature reconstructions: using in-situ estimates for thermal conductivity acquired with a fiber-optic distributed thermal perturbation sensor. Geophys Res Lett 35:L14309. https://doi.org/10.1029/2008GL034762

69. Siska P, Latal J, Bujok P, Vanderka A, Klempa M, Koudelka P et al (2016) Optical fiber based distributed temperature systems deployment for measurement of boreholes temperature profiles in the rock massif. Opt Quant Electron 48(2):108

70. Hurtig E, Großwig S, Jobmann M, Kühn K, Marschall P (1994) Fibre-optic temperature measurements in shallow boreholes: experimental application for fluid logging. Geothermics 23(4):355–364

71. Majorowicz JA, Smith SL (1999) Review of the ground temperatures in the Mallik field area: a constraint to the methane hydrate stability. Bull Geol Surv Can 544:45–56. ISSN 0068-7626

72. Roshan H, Young M, Andersen M, Acworth R (2014) Limitations of fibre optic distributed temperature sensing for quantifying surface water groundwater interactions. Hydrol Earth Syst Sci Discuss 11(7):8167–8190. https://doi.org/10.5194/hessd-118167-2014

73. Hausner MB, Suárez F, Glander KE, Giesen NVD, Selker JS, Tyler SW (2011) Calibrating single-ended fiber-optic Raman spectra distributed temperature sensing data. Sensors 11(11):10859–10879. https://doi.org/10.3390/s111110859

74. Van De Giesen N, Steele-Dunne SC, Jansen J, Hoes O, Hausner MB, Tyler S, Selker J (2012) Double-ended calibration of fiber-optic Raman spectra distributed temperature sensing data. Sensors 12(5):5471–5485. https://doi.org/10.3390/s120505471

75. Gamage DNV, Biswas A, Strachan IB, Adamchuk VI (2018) Soil water measurement using actively heated fiber optics at field scale. Sensors 18:1116. https://doi.org/10.3390/s18041116

76. Zubelzu S, Rodriguez-Sinobas L, Saa-Requejo A, Benitez J, Tarquis AM (2019) Assessing soil water content variability through active heat distributed fiber optic temperature sensing. Agric Water Manag 212:193–202

77. Benítez-Buelga J, Rodríguez-Sinobas L, Sánchez Calvo R, Gil-Rodríguez M, Sayde C, Selker JS (2016) Calibration of soil moisture sensing with subsurface heated fiber optics using numerical simulation. Water Resour Res 52(4):2985–2995

78. Liu G, Knobbe S, Butler J (2013) Resolving centimeter-scale flows in aquifers and their hydrostratigraphic controls. Geophys Res Lett 40:1098–1103. https://doi.org/10.1002/grl.50282

79. Folch A, del Val L, Luquot L, Martínez-Pérez L, Bellmunt F, Le Lay H et al (2020) Combining fiber optic DTS, cross-hole ERT and time-lapse induction logging to characterize and monitor a coastal aquifer. J Hydrol 588:125050

80. Maldaner CH, Munn JD, Coleman TI, Molson JW, Parker BL (2019) Groundwater flow quantification in fractured rock boreholes using active distributed temperature sensing under natural gradient conditions. Water Resour Res 55(4):3285–3306

81. Sebok CH, Munn JD, Coleman TI, Molson JW, Parker BL (2019) Groundwater flow quantification in fractured rock boreholes using active distributed temperature sensing under natural gradient conditions. Water Resour Res 55(4):3285–3306

82. Mateeva A, Lopez J, Potters H, Andrey J, Cox B, Kiyashchenko D et al (2014) Distributed acoustic sensing for reservoir monitoring with vertical seismic profiling. Geophys Prospect 62(Vertical seismic profiling and microseismicity frontiers):679–692

83. Dean T, Cuny T, Hartog A (2017) The effect of gauge length on axially incident P-waves measured using fibre optic distributed vibration sensing. Geophys Prospect 65:184–193

84. Kasahara J, Hasada Y, Kuzume H, Fujise Y, Mikada H, Yamamoto K (2020) Seismic feasibility study to identify and characterize supercritical geothermal reservoirs using DTS, DAS, and surface seismic array. In: Proceedings World geothermal congress

85. Bakulin A, Hemyari E, Silvestrov I (2019) Acquisition trial of DrillCAM: real-time seismic with wireless geophones, instrumented top drive and near-bit accelerometer. In: SEG Technical program expanded abstracts 2019. Society of Exploration Geophysicists, pp 157–161

86. Harris K, White D, Melanson D, Samson C, Daley TM (2016) Feasibility of time-lapse VSP monitoring at the Aquistore CO_2 storage site using a distributed acoustic sensing system. Int J Greenhouse Gas Control 50:248–260

87. Kruiver P, Obando-Hernández E, Pefkos M, Karaoulis M, Bakx W, Doornenbal P et al (2020) Fibre optic monitoring of groundwater flow in a drinking water extraction well field. In: First EAGE workshop on fibre optic sensing, vol 2020, no 1. European Association of Geoscientists & Engineers, pp 1–5

88. Ajo-Franklin JB, Dou S, Lindsey NJ, Monga I, Tracy C, Robertson M et al (2019) Distributed acoustic sensing using dark fiber for near-surface characterization and broadband seismic event detection. Sci Rep 9(1):1–14

89. Dou S, Lindsey N, Wagner AM, Daley TM, Freifeld B, Robertson M, Peterson J, Ulrich C, Martin ER, Ajo-Franklin JB (2017) Distributed acoustic sensing for seismic monitoring of the near surface: a traffic-noise interferometry case study. Sci Rep 7(1):1–12

90. Willis ME, Barfoot D, Ellmauthaler A, Wu X, Barrios O, Erdemir C et al (2016) Quantitative quality of distributed acoustic sensing vertical seismic profile data. Lead Edge 35(7):605–609

91. Shi B, Zhang D, Zhu H-H (2019) Distributed fiber optic sensing for geoengineering monitoring, 1st edn. Science Press, Beijing (in Chinese)

92. Murdoch LC, Freeman CE, Germanovich LN, Thrash C, DeWolf S (2015) Using in situ vertical displacements to characterize changes in moisture load. Water Resour Res 51(8):5998–6016

93. Zhang Y, Lei X, Hashimoto T, Xue Z (2020) In situ hydromechanical responses during well drilling recorded by fiber-optic distributed strain sensing. Solid Earth 11(6):2487–2497

94. Houizot P, Anne ML, Boussard-Pledel C, Loreal O, Tariel H, Lucas J (2014) Shaping of looped miniaturized chalcogenide fiber sensing heads for mid-infrared sensing. Sensors 14:17905–17914

95. Sanghera JS, Kung FH, Busse LE, Pureza PC, Aggarwal ID (1995) Infrared evanescent absorption-spectroscopy of toxic-chemicals using chalcogenide class fibers. J Am Ceram Soc 78:2198–2202

96. Le Coq D, Michel K, Keirsse J, Boussard-Pledel C, Fonteneaua G, Bureau B (2002) Infrared glass fibers for in-situ sensing, chemical and biochemical reactions. C R Chim 5:907–913

97. Anne ML, La Salle ELG, Bureau B, Tristant J, Brochot F, Boussard-Pledel C (2009) Polymerisation of an industrial resin monitored by infrared fiber evanescent wave spectroscopy. Sens Actuators B Chem 137:687–691

98. Brandily ML, Monbet V, Bureau B, Boussard-Pledel C, Loreal O, Adam JL (2011) Identification of foodborne pathogens within food matrices by IR spectroscopy. Sens Actuators B Chem 160:202–206

99. Jiang X, Jha A (2015) Engineering of a Ge-Te-Se glass fibre evanescent wave spectroscopic (FEWS) mid-IR chemical sensor for the analysis of food and pharmaceutical products. Sens Actuators B Chem 206:159–169

100. Anne ML, Le Lan C, Monbet V, Boussard-Pledel C, Ropert M, Sire O (2009) Fiber evanescent wave spectroscopy using the mid-infrared provides useful fingerprints for metabolic profiling in humans. J Biomed Opt 14

101. Chahal R, Starecki F, Boussard-Plédel C, Doualan JL, Michel K, Brilland L et al (2016) Fiber evanescent wave spectroscopy based on IR fluorescent chalcogenide fibers. Sens Actuators B Chem 229:209–216. https://doi.org/10.1016/j.snb.2016.01.091

102. de Frutos Cachorro J, Erdlenbruch K, Tidball M (2017) A dynamic model of irrigation and land-use choice: application to the Beauce aquifer in France. Eur Rev Agric Econ 44(1):99–120. https://doi.org/10.1093/erae/jbw005

103. Le Coz D (2000) Gestion durable d'une ressource en eaux souterraines Cas de la nappe de Beauce. La Houille Blanche 7–8:116–121. https://doi.org/10.1051/lhb/2000085

104. Ménillet F, Edwards N (200) The Oligocene–Miocene Calcaires de Beauce (Beauce limestones), Paris Basin, France. https://doi.org/10.1306/St46706C38

105. Flipo N, Monteil C, Poulin M, de Fouquet C, Krimissa M (2012) Hybrid fitting of a hydrosystem model: long-term insight into the Beauce aquifer functioning (France). Water Resour Res 48(5):W05509. https://doi.org/10.1029/2011WR011092

106. Graveline N (2020) Combining flexible regulatory and economic instruments for agriculture water demand control under climate change in Beauce. Water Resour Econ 29:100143. https://doi.org/10.1016/j.wre.2019.100143

107. Lejars C, Fusillier JL, Bouarfa S, Coutant C, Brunel L (2012) Limitation of agricultural groundwater uses in Beauce (France): what are the impacts on farms and on the food-processing sector? Irrig Drain 61:54–64. https://doi.org/10.1002/ird.1659

108. Légifrance (1992) LOI n° 92-3 du 3 janvier 1992 sur l'eau (1)

109. European Commission (2000) Directive 2000/60/EC of the European Parliament and of the council of 23 October 2000 establishing a framework for community action in the field of water policy

110. European Commission (1991) Council directive of 12 December 1991 concerning the protection of waters against pollution caused by nitrates from agricultural sources (91/676/EEC)

111. European Commission (2009) Directive 2009/128/EC of the European Parliament and of the council of 21 October 2009 establishing a framework for community action to achieve the sustainable use of pesticides

112. Vereecken H, Schnepf A, Hopmans JW, Javaux M, Or D (2016) Modeling Soil processes: review, key challenges, and new perspectives. Vadose Zone J 15(5). https://doi.org/10.2136/vzj2015.09.0131

113. Aldana C, Isch A, Bruand A, Azaroual M, Coquet Y (2021) Relationship between hydraulic properties and material features in a heterogeneous vadose zone of a vulnerable limestone aquifer. Vadose Zone J 20(4):e20127. https://doi.org/10.1002/vzj2.20127

114. Isch A, Aldana C, Coquet Y, Azaroual M (2020) Material characteristics, hydraulic properties, and water travel time through the heterogeneous vadose zone of a Cenozoic limestone aquifer (Beauce, France). EGU 2020. https://doi.org/10.5194/egusphere-egu2020-5862

115. IUSS Working Group WRB (2015) World reference base for soil resources 2014, update 2015. In: International soil classification system for naming soils and creating legends for soil maps. World Soil Resources Reports No. 106. FAO, Rome

116. Vereecken H, Huisman JA, Bogena H, Vanderborght J, Vrugt JA (2008) On the value of soil moisture measurements in vadose zone hydrology: a review. Water Resour Res 44(4):W00D06. https://doi.org/10.1029/2008WR006829

117. Whalley WR, Ober ES, Jenkins M (2013) Measurement of the matric potential of soil water in the rhizosphere. J Exp Bot 64(13):3951–3963. https://doi.org/10.1093/jxb/ert044

118. Lekshmi SUS, Singh DN, Baghini MS (2014) A critical review of soil moisture measurement. Measurement 54:92–105. https://doi.org/10.1016/j.measurement.2014.04.007

119. Nolz R (2016) A review on the quantification of soil water balance components as a basis for agricultural water management with a focus on weighing lysimeters and soil water sensors. J Land Manag Food Environ 67(3). https://doi.org/10.1515/boku-2016-0012

120. Singh G, Kaur G, Williard K, Schoonover J, Kang J (2018) Monitoring of water and solute transport in the vadose zone: a review. Vadose Zone J 17(1):23. https://doi.org/10.2136/vzj2016.07.0058

121. Šimůnek J, van Genuchten MTh, Šejna M (2016) Recent developments and applications of the HYDRUS computer software packages. Vadose Zone J 15(7):25. https://doi.org/10.2136/vzj2016.04.0033

122. Isch A, Coquet Y, Aldana C, Bruand A, Azaroual M (2021) Simulation of water flow and estimation of travel time through the heterogeneous vadose zone of a vulnerable limestone aquifer based on laboratory hydraulic properties measurements. Manuscript submitted for publication in J Hydrol (under review)

123. Wellings SR, Bell JP (1980) Movement of water and nitrate in the unsaturated zone of Upper Chalk near Winchester, Hants., England. J Hydrol 48(1):119–136. https://doi.org/10.1016/0022-1694(80)90070-0

124. McLing TL, Brandon W, Zavata B, Smith RW, Smith C (2017) The application of radon for mapping open fracture networks in a thin vadose zone. Vadose Zone J 16(7). https://doi.org/10.2136/vzj2016.11.0116

125. Isch A, Azaroual M (2019) Fluids transfers and hydrodynamics of the Vadose Zone of the O-ZNS platform site. In: Knowledge's frontiers in water unsaturated hydrogeosystems: interface dynamics, heterogeneities & couplings, Orléans

126. Abbar B, Isch A, Azaroual MM (2020) Fiber optic and hydrogeological sensors for the monitoring of mass and heat transfers through the vadose zone of a Cenozoic limestone aquifer (Beauce, Orléans, France). In: AGU Fall meeting

127. Abbar B, Jodry C, Isch A, Laurent G, Azaroual M (2020) Monitoring of the mass and heat transfers through a heterogeneous karstic limestone vadose zone of an agricultural field (Beauce aquifer, Orleans, France), EGU 2020-5294. Virtual, 3–8 May 2020. https://doi.org/10.5194/egusphere-egu2020-5294

128. Pütz T, Fank J, Flury M (2018) Lysimeters in vadose zone research. Vadose Zone J 17(1):180035. https://doi.org/10.2136/vzj2018.02.0035

129. Isch A, Montenach D, Hammel F, Ackerer P, Coquet Y (2019) A comparative study of water and bromide transport in a bare loam soil using lysimeters and field plots. Water 11(6):1199. https://doi.org/10.3390/w11061199

130. Weihermüller L, Siemens J, Deurer M, Knoblauch S, Rupp H (2007) In situ soil water extraction: a review. J Environ Qual 36(6):1735–1748. https://doi.org/10.2134/jeq2007.0218

131. Dahan O, Talby R, Yechieli Y, Adar E, Lazarovitch N (2009) In situ monitoring of water percolation and solute transport using a vadose zone monitoring system. Vadose Zone J 8(4):916. https://doi.org/10.2136/vzj2008.0134

132. Quinn P, Parker BL, Cherry JA (2015) Blended head analyses to reduce uncertainty in packer testing in fractured-rock boreholes. Hydrogeol J 24(1):59–77. https://doi.org/10.1007/s10040-015-1326-2